Science Advances
AAAS

Supplementary Materials for

Structural insights into the calcium-coupled zinc export of human ZnT1

Chunqiao Sun *et al.*

Corresponding author: Xingbing Wang, wangxingbing@ustc.edu.cn; Xin Liu, lx023@ustc.edu.cn; Linfeng Sun, sunlf17@ustc.edu.cn

Sci. Adv. **10**, eadk5128 (2024)
DOI: 10.1126/sciadv.adk5128

This PDF file includes:

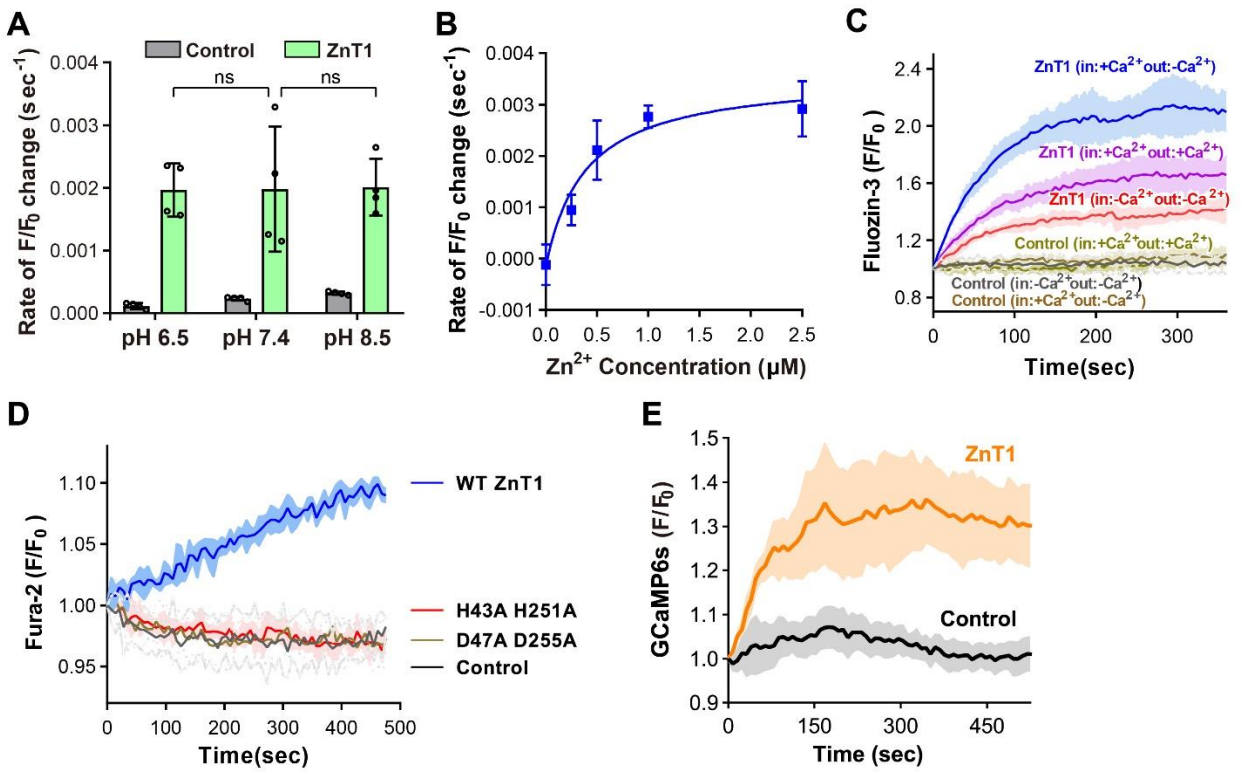

Fig. S1. Characterizations of the zinc transport activity of hZnT1.

(**A**) Comparison of the initial rates of fluorescence change of FluoZin-3 AM due to Zn^{2+} efflux in HEK293T cells in the assay buffer of different pH. Each data point represents the initial rate calculated from the mean of fluorescence changes of at least ten cells from one coverslip, and the experiment was repeated four times with four independent coverslips. significances were determined using a two-tailed unpaired *t*-test. ns = not significant. Data are means ± SD. (**B**) Initial rates of Zn^{2+} influx are plotted against the Zn^{2+} concentration, and fitted with the Hill equation. Each data point is mean of four independent measurements. Data are means ± SD. (**C**) Zn^{2+} efflux by hZnT1 measured by the fluorescence change (F/F_0) of FluoZin-3 in the proteoliposome-based transport assay in the presence or absence of a transmembrane Ca^{2+} gradient as indicated. Fluorescence traces are shown as solid line (mean) with shaded areas (standard deviation, SD) from at least three biological repeats. (**D**) Ca^{2+} transport by the wild-type (WT) hZnT1 and the mutants as measured by the fluorescence change (F/F_0) of Fura-2 in the proteoliposome-based transport assay. Fluorescence traces are shown as solid line (mean) with shaded areas (standard deviation, SD) from at least three biological repeats. (**E**) Ca^{2+} influx by hZnT1 as measured by the proteoliposome-based assay using GCaMP6s as the indicator. Fluorescence changes (F/F_0) of GCaMP6s are compared for proteoliposomes loaded with WT hZnT1 (orange) and protein-unloaded liposomes (black). Fluorescence traces are shown as solid line (mean) with shaded areas (standard deviation, SD) from at least three repeats.

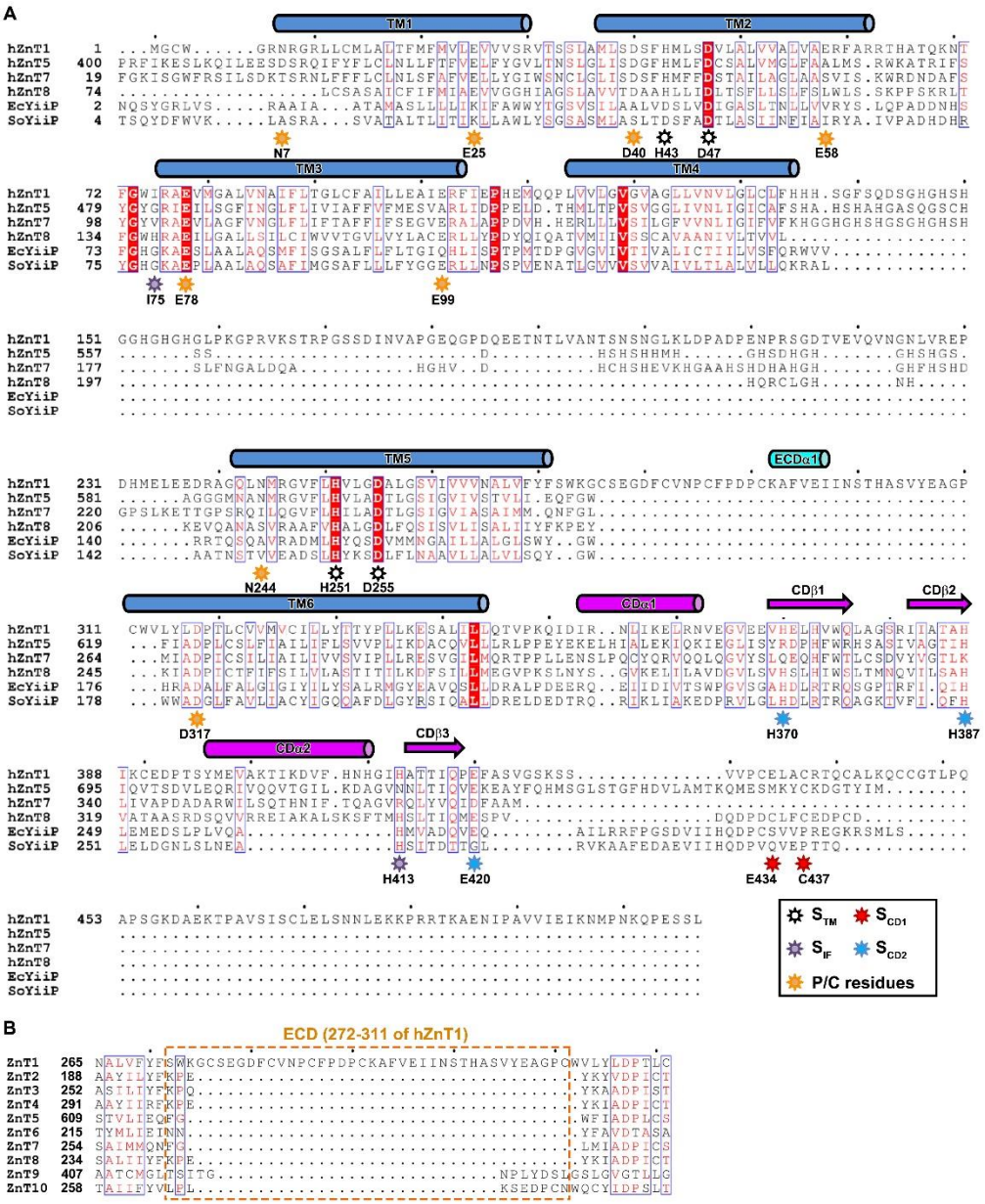

Fig. S2. Sequence alignments of the human ZnTs, *Ec*YiiP and *So*YiiP.

(**A**) Sequences for hZnT1, hZnT5, hZnT7, hZnT8, *Ec*YiiP and *So*YiiP are publicly available at Uniprot (https://www.uniprot.org) with the following accession codes: hZnT1: Q9Y6M5, hZnT5: Q8TAD4, hZnT7: Q8NEW0, hZnT8: Q8IWU4, *Ec*YiiP: P69380, and *So*YiiP: Q8E919. Sequences are aligned using ClustalW. Secondary structural elements of hZnT1 as identified in the high-resolution hZnT1-DM structure are indicated above the sequence. Invariant amino acids are shaded red. The putative zinc binding residues in S_{TM}, S_{IF}, S_{CD1} and S_{CD2}, and the critical polar or negatively-charged (P/C) residues in the metal translocation pathway are indicated by stars in different colors. (**B**) Sequence alignments of the ECD region in human ZnTs. Sequences for hZnT1-10 are publicly available at Uniprot (https://www.uniprot.org). The corresponding sequences to the ECD region in hZnT1 (shown in the orange box with dashed lines) are unconserved and much shorter in other hZnTs.

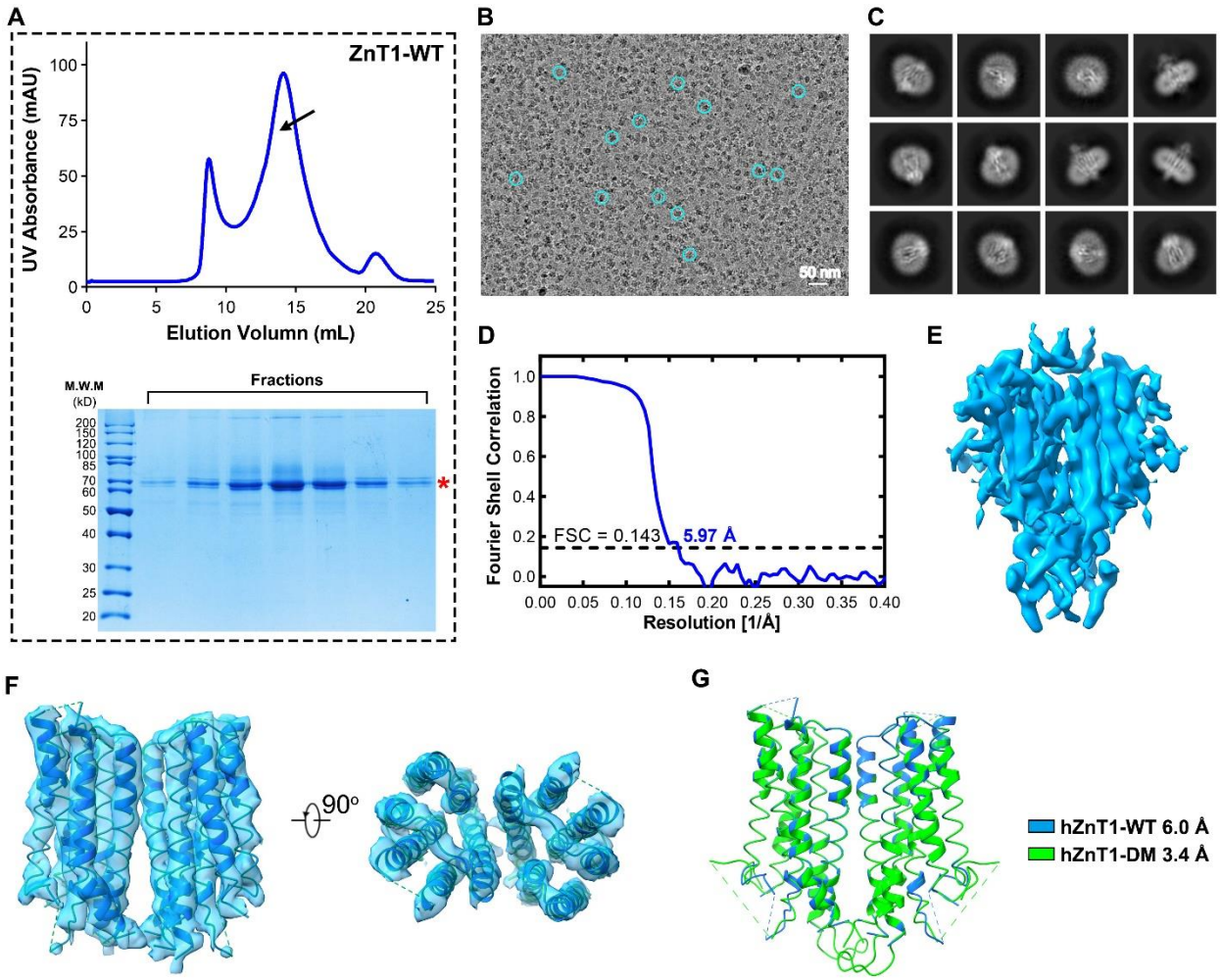

Fig. S3. Cryo-EM analysis of the wild-type hZnT1 protein.

(**A**) Representative gel filtration analysis of the WT hZnT1 protein. The mono-disperse peak of the protein indicated by the arrow and verified by Coomassie-blue-staining SDS-PAGE, suggests a good solution behavior of the sample. (**B**) A typical cryo-EM image of the WT hZnT1 sample. Representative particles are indicated by circles in cyan. (**C**) Typical 2D classification images of the WT hZnT1. (**D**) The gold-standard Fourier shell correlation (FSC) curve for the EM map of the WT hZnT1. The resolution reaches 6.0 Å by a threshold of 0.143. (**E**) 3D reconstruction map of the WT hZnT1 at an overall resolution of 6.0 Å. (**F**) Structure model for the transmembrane domain of the WT hZnT1. (**G**) Structure comparison for the transmembrane domain of the WT ZnT1 and the ZnT1-DM mutant.

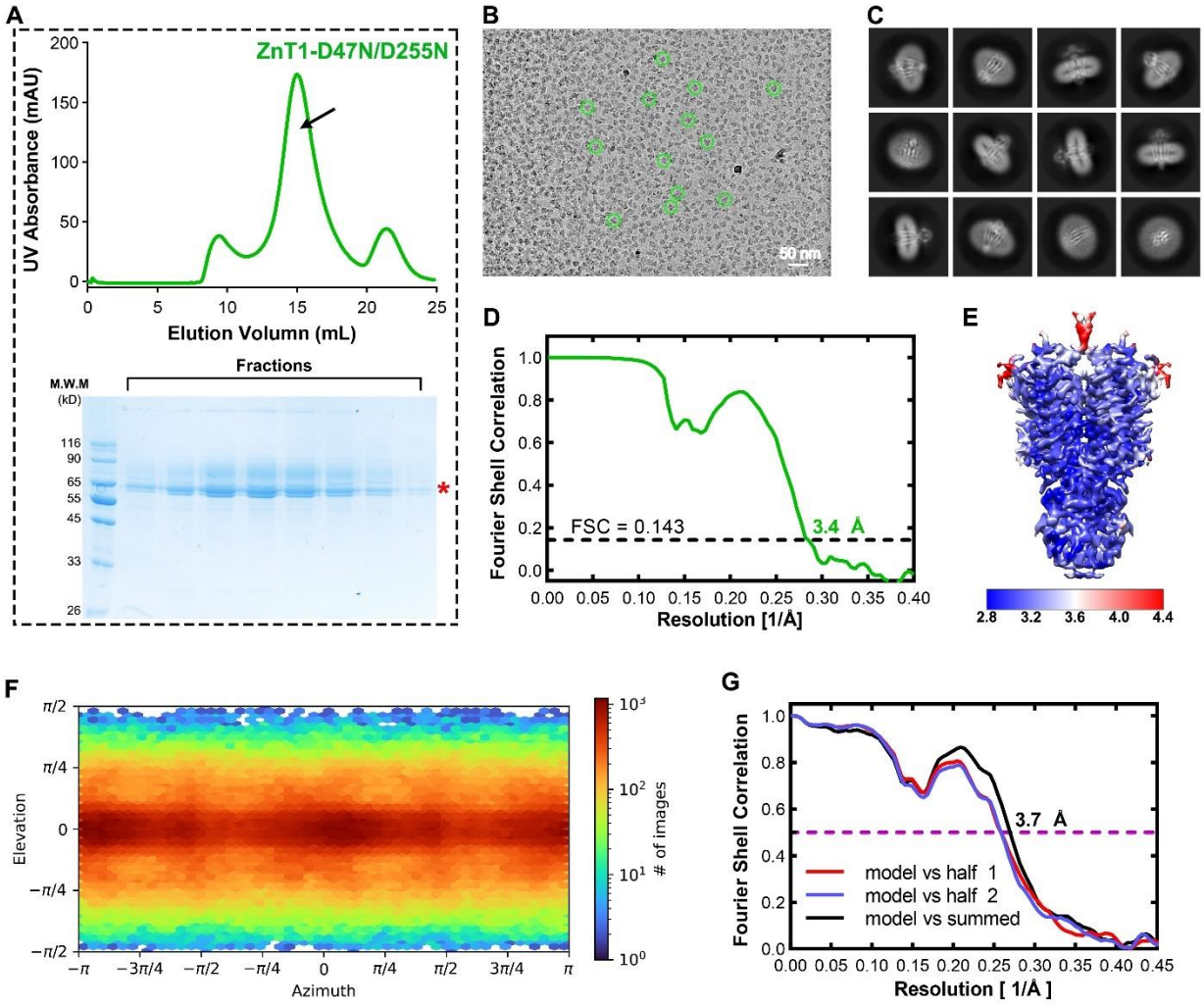

Fig. S4. Cryo-EM analysis of the hZnT1-DM protein.

(**A**) Representative gel filtration and Coomassie-blue-staining SDS-PAGE results of hZnT1-DM. (**B**) A typical cryo-EM image of the hZnT1-DM. (**C**) Typical 2D classification images of the hZnT1-DM. (**D**) The gold-standard Fourier shell correlation curve for the overall map of the hZnT1-DM. The resolution reaches 3.4 Å by a threshold of 0.143. (**E**) The local resolution maps of hZnT1-DM sample calculated using ResMap. (**F**) Euler angle distribution of the hZnT1-DM images as calculated in cryoSPARC. (**G**) FSC model curves of the hZnT1-DM map.

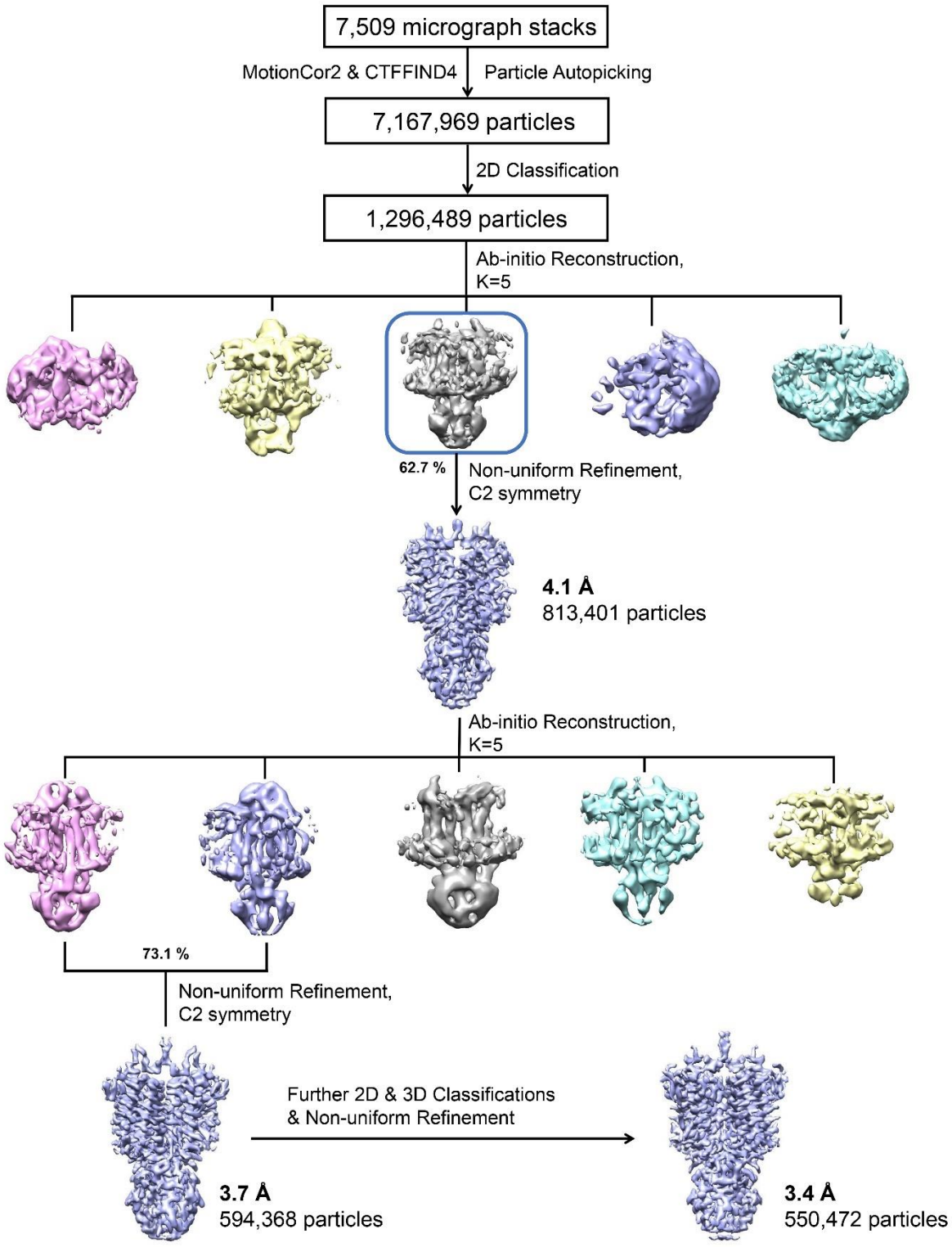

Fig. S5. Flowchart for the cryo-EM data processing of hZnT1-DM.
Details can be found in the "Image processing" session in the Materials and Methods.

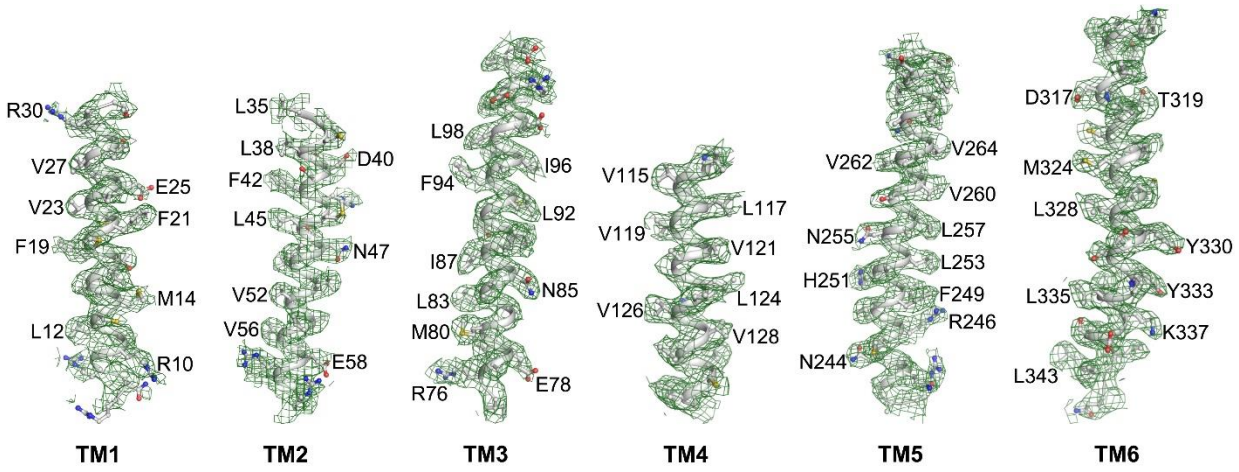

Fig. S6. Representative EM densities for the transmembrane helices of hZnT1-DM structure.
EM densities for the six TMs of hZnT1-DM are shown in green mesh. Residues with large notable side chains are labeled aside.

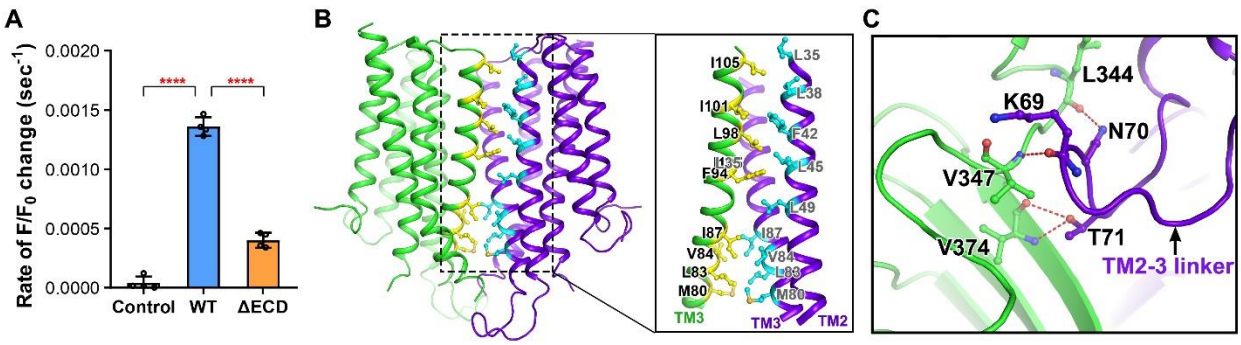

Fig. S7. Characterization of the ECD domain and the dimer interface of hZnT1.

(**A**) Initial fluorescence change rates for the WT hZnT1 and ΔECD mutant as measured by the proteoliposome-based Zn^{2+} transport assay using FluoZin-3. Independent experiments were repeated four times for each construct. Data are means ± SD. Significances were determined using one-way ANOVA with Dunnett's multiple comparisons test. **** $P < 0.0001$. (**B**) The dimer interface of hZnT1-DM in the transmembrane domain. (**C**) Interactions between the β-sheets of one protomer and the TM2-TM3 linker of another protomer.

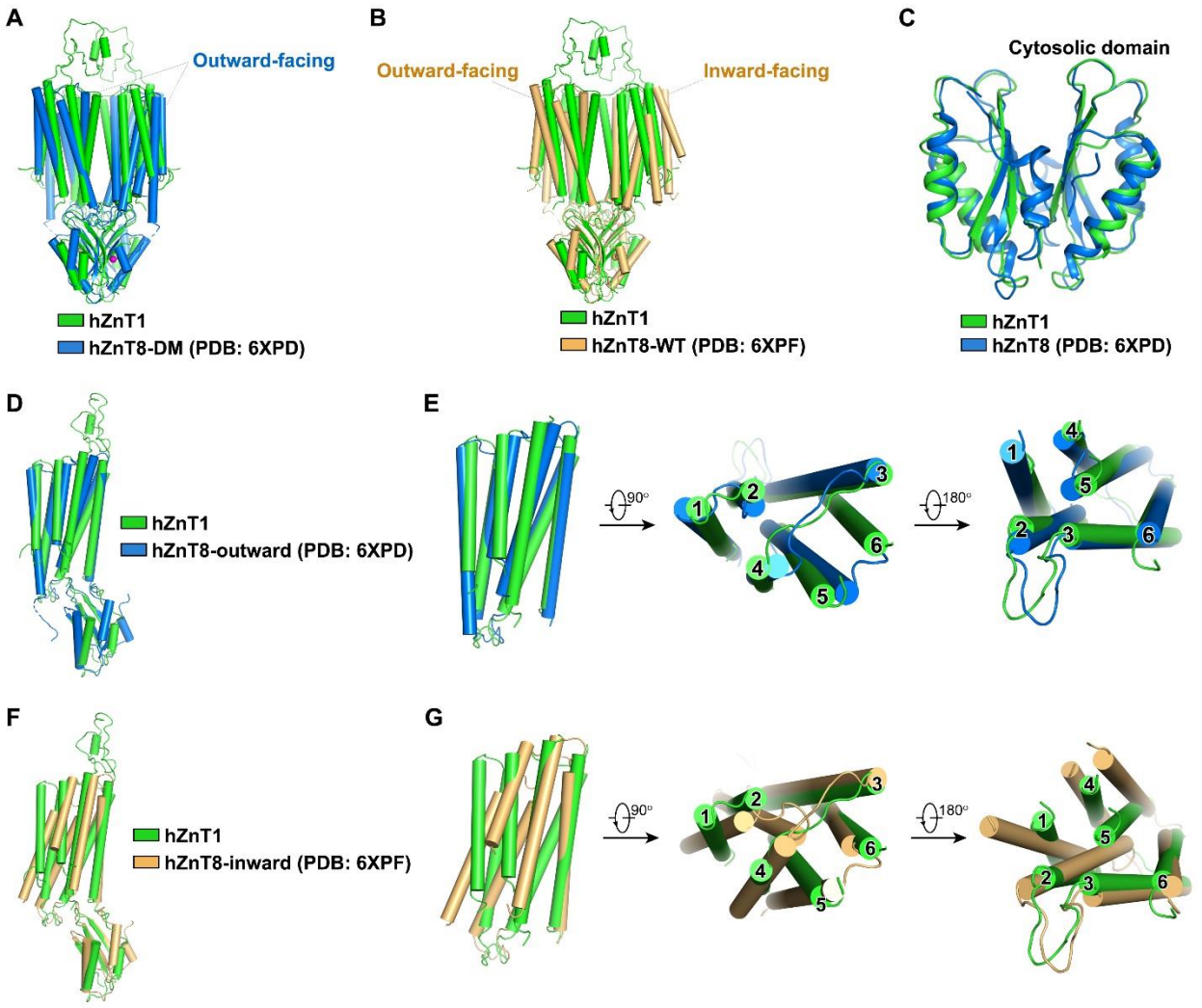

Fig. S8. Structural comparisons between hZnT1-DM and hZnT8.

(**A**) Structure alignment between the hZnT1-DM dimer and the outward-facing structure of hZnT8-DM dimer (PDB code: 6XPD). (**B**) Structure alignment between the hZnT1-DM dimer and the WT hZnT8 dimer in heterogeneous states (PDB code: 6XPF). (**C**) Structure alignment of the cytosolic domains of hZnT1-DM and hZnT8-DM (PDB code: 6XPD). (**D**) Structural alignment between the monomeric hZnT1-DM and the outward-facing hZnT8-DM monomer (PDB code: 6XPD). (**E**) Superposition of the transmembrane domains alone from hZnT1-DM and hZnT8-DM in the outward-facing state (PDB code: 6XPD). (**F**) Structural alignment between the monomeric hZnT1-DM and the inward-facing WT hZnT8 monomer (PDB code: 6XPF). (**G**) Superposition of the transmembrane domains alone from hZnT1-DM and the inward-facing WT hZnT8 (PDB code: 6XPF).

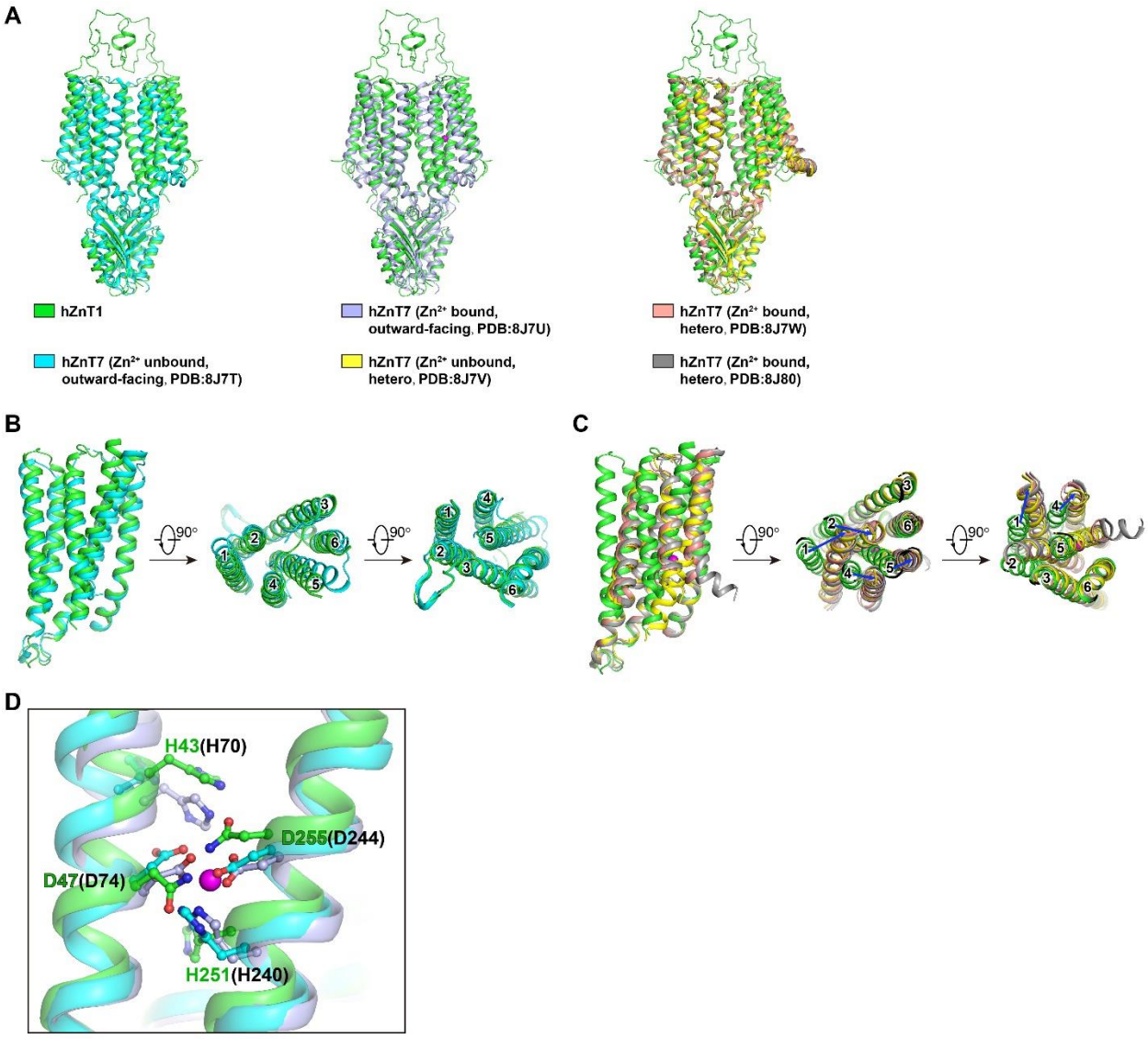

Fig. S9. Structural comparisons between hZnT1-DM and hZnT7.

(**A**) Structure alignment between the hZnT1-DM dimer and hZnT7 dimer under different states. (**B**) Superposition of the transmembrane domains alone from hZnT1-DM and hZnT7 in the outward-facing state (PDB code: 8J7T). (**C**) Superposition of the transmembrane domains alone from hZnT1-DM and hZnT7 in the heterogeneous states (PDB code: 8J7V, 8J7W and 8J80). (**D**) Superposition of the S_{TM} Zn^{2+} binding sites between hZnT1-DM (green) and outward-facing hZnT7 structures. Residues forming the binding site in hZnT1 are shown in sticks with carbon atoms colored green, in the Zn^{2+}-unbound, outward-facing structure of hZnT7 colored cyans (PDB code: 8J7T), and in the Zn^{2+}-bound, outward-facing structure of hZnT7 colored light blue (PDB code: 8J7U). The same color scheme is used in (**A** to **D**), as indicated in (**A**).

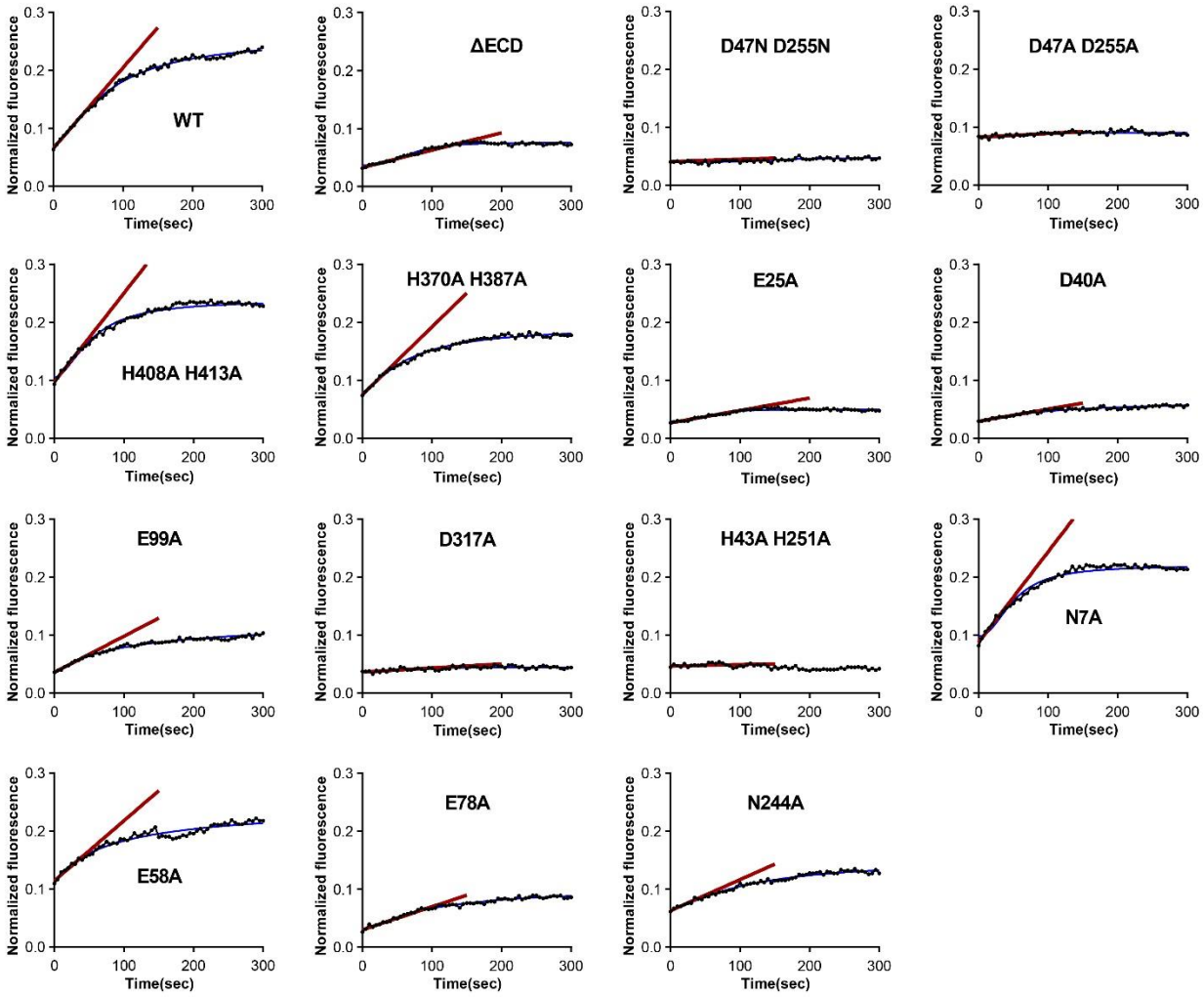

Fig. S10. Representative normalized fluorescence curves as measured in the proteoliposome-based Zn^{2+} transport assay using FluoZin-3 for the WT hZnT1 and its mutants.

For normalization, the maximal fluorescence intensity was measured after solubilizing the Fluozin-3-containing liposome (FL_{max}) or proteoliposomes (FP_{max}) with 4% octyl-β-D-glucoside detergent solution containing 64 mM $ZnCl_2$. Zn^{2+} transport activity was then calculated using the equation (FP/FP_{max}) - (FL/FL_{max}) over time. FP, fluorescence counts of proteoliposomes; FL, fluorescence counts of liposome; FP_{max}; maximal fluorescence counts of proteoliposomes; FL_{max}, maximal fluorescence counts of liposomes. After subtracting the fluorescence signals of the empty liposome from those of proteoliposomes, the normalized fluorescence curve of the WT hZnT1 or the mutants was fitted by a single exponential function (blue line), respectively. Values of the initial Zn^{2+} uptake were then calculated (brown line).

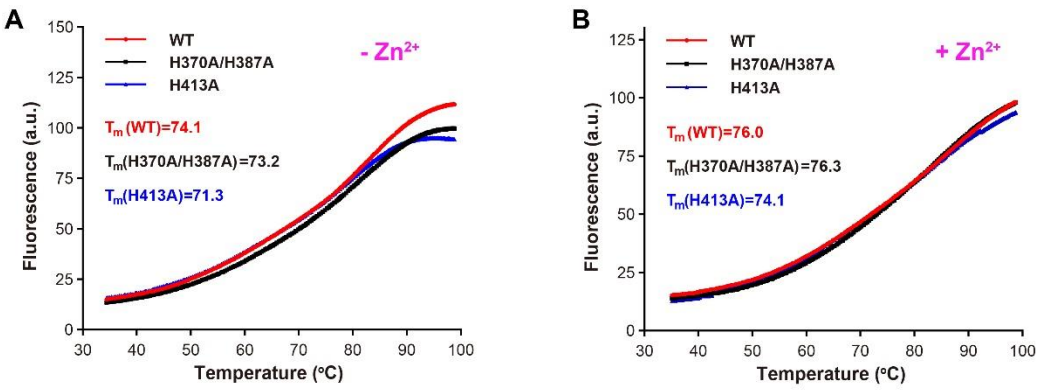

Fig. S11. Characterizations of the thermal stability for the WT hZnT1 and its mutants.

(**A**) Microscale fluorescent based thermal stability assay result for the WT hZnT1 and mutants in the S_{CD2} and S_{IF} Zn^{2+} binding sites in the absence of Zn^{2+}. Calculated T_m values for the mutants are shown. (**B**) Microscale fluorescent based thermal stability assay result for the WT hZnT1 and mutants in the S_{CD2} and S_{IF} Zn^{2+} binding sites in the presence of Zn^{2+}.

Table S1. Statistics of cryo-EM data collection, processing, model refinement and validation.

Data Collection	**hZnT1-D47N/D255N**
EM equipment	FEI Titan Krios
Voltage (kV)	300
Detector	Gatan BioQuantum K3
Pixel size (Å)	1.1
Electron dose (e^-/Å^2)	50
Defocus range (μm)	-1.5 ~ -2.3
3D Reconstruction	
Software	RELION, cryoSPARC
Number of Particles	550,472
Symmetry	C2
Map Resolution (Å)	3.4
FSC Threshold	0.143
Model Refinement	
Map Sharpening B-factor (Å^2)	-227.6
Model Resolution (Å)	3.7
FSC Threshold	0.5
Protein residues	650
Side chains	650
Ligands	0
CC mask	0.80
Validation	
R.m.s. Deviations	0.01
Bond lengths (Å)	0.01
Bond angles (°)	1.405
MolProbity Score	1.69
All-atom Clashscore	3.23
Rotamer Outliers (%)	0.00
Ramachandran plot	
Favored (%)	88.94
Allowed (%)	11.06
Outliers (%)	0.00